Annals of Biomedical Engineering, Vol. 44, No. 4, April 2016 (© 2015) pp. 886–894
DOI: 10.1007/s10439-015-1408-2

Motile Human Neutrophils Sense Ligand Density Over Their Entire Contact Area

STEVEN J. HENRY,[1] JOHN C. CROCKER,[2] and DANIEL A. HAMMER[1,2]

[1]Department of Bioengineering, University of Pennsylvania, 240 Skirkanich Hall, 210 S. 33rd St., Philadelphia, PA 19104, USA; and [2]Chemical and Biomolecular Engineering, University of Pennsylvania, Philadelphia, PA, USA

(*Received 7 May 2015; accepted 22 July 2015; published online 29 July 2015*)

Associate Editor Konstantinos Konstantopoulos oversaw the review of this article.

Abstract—Neutrophils are key components of the immune system and motility is central their function during the inflammatory response. We have previously demonstrated that neutrophils are capable of switching their motile phenotype between amoeboid-like and keratocyte-like in response to the ligand density of adhesion molecules (Henry *et al.* in Int Biol 6:348–356, 2014). In this study, we engineered planar micropatterned surfaces that presented adhesion molecules in local islands of high density, separated by regions largely devoid of ligands. By controlling the geometry of islands we made arrays in which the local (on island) adhesion density was high but the global (multi-island) adhesion density over the entire cell-substrate interface was low. Neutrophils in contact with these island arrays assumed a well-spread and directionally-persistent motile phenotype (keratocyte-like) in contrast to the classical amoeboid morphology they display on uniform fields of high adhesion density. By virtue of our rationally designed substrates, we were able to conclude that neutrophils were integrating the stimulation received across their entire contact interface; furthermore, they were able to mount this whole cell response on the timescale of seconds. This work demonstrates the capacity of adhesive microenvironments to direct the phenotype of cell motility, which has broader implications in physiologic processes such as inflammation and cancer metastasis.

Keywords—Motility, Haptokinesis, Amoeboid, Keratocyte, Microcontact printing, Adhesion.

INTRODUCTION

Neutrophils are white blood cells (leukocytes) that respond to tissue trauma and infection on the timescale of seconds and minutes. These cells are equipped with an arsenal of infection-fighting tools including phagocytosis, cytokine secretion, and nuclear-extracellular-trap setting.[3] A prerequisite to the execution of any of these functions is the cell's arrival at the locus of trauma[19] or infection[20] *via* vascular rolling, extravasation, and extravascular migration.[18] In addition to soluble chemical cues that direct immune cell response and function, cells encounter numerous physical cues (e.g., stiffness, dimensionality, adhesivity, and topology) that are strong determinants of shape, force generation, and gene expression.[5,27] Leukocyte response to physical cues such as substrate rigidity,[13,21,25] confinement,[14] and adhesion density[12] have been areas of on-going investigation.

It has been shown that neutrophil contact area and force generation on planar (2D) substrates is dependent on substrate stiffness.[13,21,25] However, we showed that stiffness alone was not a unique controller of adherent neutrophil shape or motility, as varying the adhesivity of the surface also dictated cell phenotype on substrates of equal stiffness.[12] In that work, using the method of microcontact printing, we quantified neutrophil shape and motility on sub-saturating densities of the extracellular matrix protein fibronectin (FN). On high densities of FN, neutrophils assumed a classic amoeboid phenotype characterized by an elongated cell body, knob-like trailing uropod, and a narrow, ruffled leading edge lamellipodium.[4,32] The observed motility was fast and consisted of frequent directional changes. However, on surfaces presenting low or intermediate FN density, neutrophils assumed a phenotype reminiscent of fish keratocytes,[2,16] characterized by the absence of a trailing uropod and a highly spread fan-like lamellipodium. The observed motility was a slow, directionally-persistent gliding motion.

Address correspondence to Daniel A. Hammer, Department of Bioengineering, University of Pennsylvania, 240 Skirkanich Hall, 210 S. 33rd St., Philadelphia, PA 19104, USA. Electronic mail: hammer@seas.upenn.edu

The capacity of adhesion density to alter the phenotypic mode of neutrophil migration drew analogy with adhesion sensitivity in fish keratocytes observed by Barnhart *et al.*[2] and computational predictions of the effect of adhesion on stiff substrates in migratory cells made by Ziebert and Aranson.[31] Thus, we refer to this phenotype as "keratocyte-like."

An open question from our prior work was the length scale over which the neutrophil adhesion density sensing was occurring. Were neutrophils responding to local adhesive cues on the length scale of receptor clusters or integrating adhesive stimulation across their entire contact interface? To address this question we employed the stamp-off variation of microcontact printing,[10] to generate a hybrid surface in which high and low density adhesive cues were presented to neutrophils simultaneously. This engineering approach of spatially organizing a cell's adhesive environment has been widely used to probe integrin clustering,[1,9] the effect of cell shape on viability[7] and focal adhesion architecture,[6] and the role of extracellular matrix distribution on cell spreading[17] in mesenchymal cells. Here we report the effect of adhesive ligand distribution on neutrophil motility, and show that neutrophils can respond to ligand presentation across their entire contact interface.

MATERIALS AND METHODS

Media and Reagents

Rinsing buffer was Hanks' Balanced Salt Solution (Life Technologies, Carlsbad, CA) without calcium or magnesium supplemented with 10 mM HEPES (Life Technologies) and pH adjusted to 7.4. Storage buffer was rinsing buffer supplemented with 2 mg/mL glucose. Running buffer was storage buffer supplemented with 1.5 mM Ca^{2+} and 2 mM Mg^{2+}. Fibronectin (FN) was from human plasma (BD Biosciences, Bedford, MA). Labeling of FN *via* Alexa Fluor carboxylic acid, succinimidyl ester (Life Technologies) was performed in accordance with the manufacturer's recommended protocol. The nonionic triblock copolymer Pluronic F-127 (Sigma) was prepared at 0.2% w/v in PBS without calcium and magnesium (PBS(-)). All solutions were sterile filtered or prepared sterile. The bicinchoninic acid protein assay (Pierce Biotechnology, Rockford, IL) was performed on stock FN solutions to measure concentration. Poly(dimethylsiloxane) (PDMS) was Sylgard 184 Silicone Elastomer from Dow Corning (Midland, MI) prepared per the specified weight ratio of base:cure agents, mixed vigorously, and degassed until optically clear.

Substrate Production

25:1 base:cure (w/w) PDMS stamps were cast against a silicon wafer to produce an extremely smooth surface. Stamps were trimmed to approximately 25 mm^2, sonicated in 200 proof ethanol for 10 min, rinsed twice in diH_2O and dried in a gentle stream of filtered $N_{2(g)}$. The surface of the PDMS stamp, previously cast against the silicon wafer, was incubated with a 50 μL aliquot of fluorescently labeled FN (FN-AlexaFluor594) at a known concentration in PBS(-) for 1 h at room temperature. After incubation stamps were rinsed twice in a submerging quantity (~50 mL) of diH_2O and dried in a gentle stream of filtered $N_{2(g)}$ (Fig. 1a).

For experiments with islands, inked stamps were subject to stamp-off. An array of holes was generated by casting 10:1 base:cure (w/w) PDMS reliefs of positive silicon microfabricated-post-array-detectors. Silicon masters were manufactured in Professor Christopher S. Chen's laboratory in the manner detailed by Yang *et al.*[29] Cast PDMS hole arrays were rendered hydrophilic by 7 min treatment in ultraviolet ozone (UVO Cleaner Model 342, Jelight, Irvine, CA).[10] The hydrophilic array was inverted, set atop the inked stamp, and peeled to produce two complimentary surfaces (Fig. 1b).

PDMS coated coverslips were prepared from number one thickness glass coverslips (Fisher Scientific, Hampton, NH) of 25 mm diameter spun with degassed PDMS [10:1 base:cure (w/w)]. Bare glass coverslips were cleaned *via* oxygen plasma etching and then spun at 4000 rpm for 1 min under PDMS. Leveling at RT, and baking at 65 °C overnight resulted in an approximately 10 μm thick layer of PDMS. Cured coverslips were affixed to the bottom of six-well tissue culture plates which had either been hot-punched or laser-cut to generate a 22 mm diameter opening in the bottom of the wells. Coverslips were bonded using Norland Optical Adhesive 68 (Thorlabs, Newton, NJ). Mounted coverslips were rendered hydrophilic by 7 min treatment in ultraviolet ozone and then printed with a continuous field of protein or the stamped-off array of islands (Fig. 1c). Substrates were blocked against nonspecific binding by submerging in 0.2% w/v F-127 in PBS(-) and incubating 30 min at RT (Fig. 1d). After blocking, F-127 was exchanged for PBS(-) by repeated and gentle rinsing with running buffer. Chambers were pre-warmed to 37 °C in a cabinet incubator before cell plating and imaging.

Neutrophil Isolation

Whole blood was obtained from human donors *via* venipuncture. Samples were collected with University

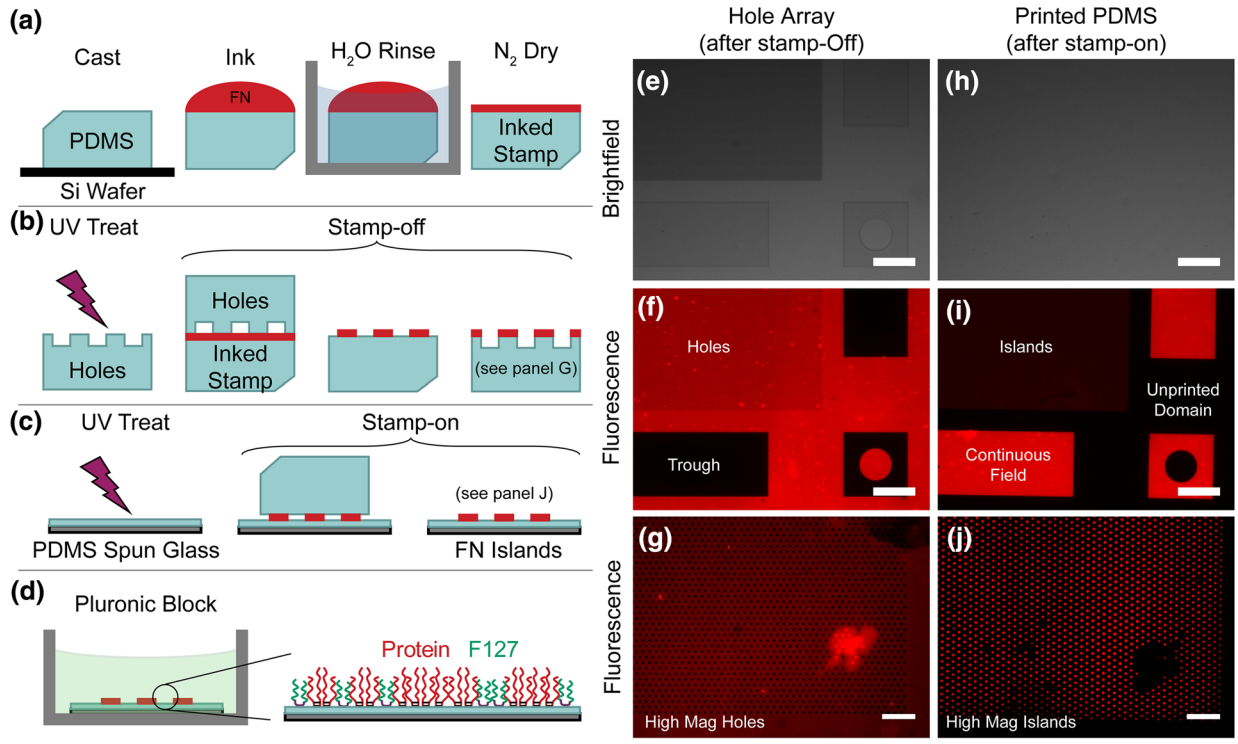

FIGURE 1. Stamp-off method of microcontact printing to generate island arrays. Substrate preparation consisted of: (a) stamp inking, (b) stamp-off, (c) stamp-on, and (d) Pluronic F-127 blocking. (e) Brightfield image of hole array used in stamp-off procedure. (f) Fluorescence image of protein on hole array after stamp-off. (g) Higher magnification image of interstitial protein on hole array after stamp-off. (h) Brightfield image of PDMS coverslip after stamp-on. (i) Fluorescence image of protein after stamp-on. (j) Higher magnification image of island array after stamp-on. Fluorescence images were contrast-enhanced to aid in visualization. Unenhanced images are reported in Electronic Supplementary Material Fig. S1. Scale bars = 200 μm for e, f, h, and i. Scale bars = 10 μm for g and j.

of Pennsylvania Institutional Review Board approval from consenting adult volunteers. Volunteers were required to be in good health and abstain from alcohol and all over-the-counter medication for 24 h prior to donation. Blood samples were allowed to cool to RT for 15 min and layered in a 1:1 ratio of whole blood to Polymorphprep (Axis-Shield, Oslo, Norway). Vials were spun for 45–60 min at 550–650×*g* and 21 °C. After separation, the polymorphonuclear band and underlying separation media layer were aspirated into fresh round-bottom tubes. The solution of cells and separation-media was diluted with rinsing buffer and spun for 10 min at 250×*g* and 21 °C. Red blood cells (RBC) were eliminated from the resulting cell pellet *via* hypotonic lysis. After lysis, vials were centrifuged for 10 min at 250×*g* and 21 °C and the RBC-free pellets resuspended in storage buffer. Neutrophils were stored at 10^6 cells/mL on a tube rotisserie at 4 °C until time of plating to maintain cells in suspension.

Quantitative Fluorescence Microscopy

A non-flickering mercury bulb within the manufacturer-specified bulb lifetime was used to illuminate samples. Adjustments to bulb alignment and focus were made to achieve a uniform field of illumination. Within a given experimental series all acquisition parameters were held constant and images acquired identically. For each condition (i.e., feature and ligand density combination) multiple fields of view (FOV) were acquired across the entire printed domain as well as appropriate measurements of background fluorescence intensity. To mitigate the effects of photobleaching, focus was set in a region adjacent to the FOV actually imaged. To compare results across independent experiments, mean fluorescent intensities were normalized by the mean intensity of the saturating condition within that series after background subtraction. Further details regarding island size and intensity quantification are provided in the Electronic Supplementary Material.

Cell Motility Experiments and Data Analysis

Neutrophils were seeded into pre-warmed culture dishes and allowed to gravity sediment onto the printed arrays. Multiple position time-lapse videomicroscopy was performed to track cell shape and position for at least 30 min with images acquired every

15–60 s. Motility quantification was performed using a custom suite of MATLAB (The MathWorks, Natick, MA) scripts which identified cell boundaries, computed geometric centroids, and connected centroids in consecutive frames to form trajectories. Cell tracking, mean squared displacement computation, and error analysis were based upon the multiple particle tracking method reviewed by Crocker and Hoffman.[8]

RESULTS

Engineering Substrates to Present Neutrophils with Two Adhesive Length Scales

By using the stamp-off method of microcontact printing (Figs. 1a–1d) we generated hexagonal arrays of submicron diameter islands of the extracellular matrix protein fibronectin (FN) (Figs. 1i and 1j). A spread neutrophil was in contact with many of these islands (~100 islands/cell) at once as they were small and tightly spaced relative to the total size of the cell (Fig. 3e). To aid visualization of the islands, contrast was enhanced in fluorescence images of Fig. 1. The unenhanced images are provided in Electronic Supplementary Material Fig. S1. Printed islands were arranged hexagonally with a measured mean diameter of 0.834 ± 0.055 μm (Fig. S4) and pitch of 1.932 ± 0.002 μm (Fig. S5). Quantities are mean ± standard error of the mean for five independent substrates with an average of 1296 printed islands measured per substrate. Individual islands had a surface area of 0.55 ± 0.07 μm^2 whereas the macroscopic surface area (i.e., a region containing many islands) represented a reduced contact area of 17 ± 2% compared to a uniformly coated field (Fig. S8).

The principal aim of this study was to generate a hybrid surface in which neutrophils were presented simultaneously with two length scales of adhesive stimulation. This required controlling array geometry and protein loading density such that the final printed surface had locally high protein content (i.e., on islands) but globally low average protein content (i.e., the area equivalent to a cell body). Inking concentration was a more facile variable to manipulate as compared to island geometry. Therefore, we fixed array geometry and performed experiments at many different concentrations to identify conditions such

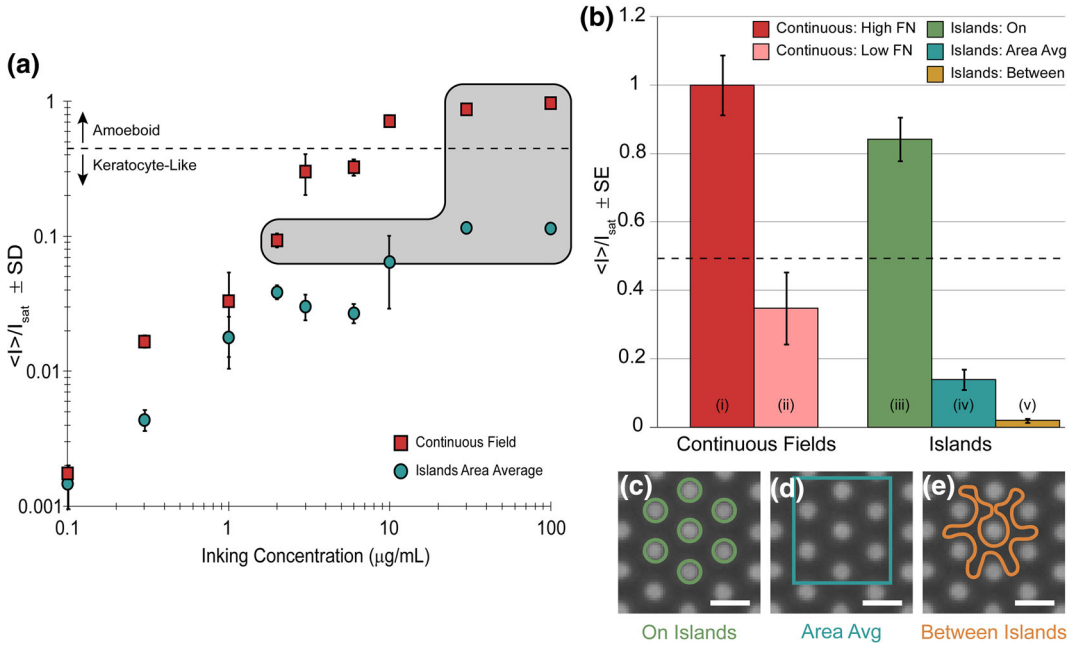

FIGURE 2. Engineering islands with two adhesive length scales. (a) Mean fluorescence intensity in field of view normalized by mean intensity at saturation ($<I>/I_{sat}$) as a function of stamp inking concentration for continuous fields (red squares) and stamped-off islands (blue circles). Gray shaded region represents domain where stamp-off of high density continuous fields produces islands with an area average equivalent to a low density continuous field. Dotted line denotes adhesive threshold delineating neutrophil phenotypes. Error bars are ± standard deviation from 2 to 4 replicates for each concentration within a single experiment. (b) Relative protein content of (i) high density FN (50 μg/mL) continuous fields, (ii) low density (2 μg/mL) continuous fields, (iii) on islands (see ROI of c), (iv) the area average of protein density across islands (see ROI of d), and (v) the residual protein density between islands (see ROI of e). Measurements corresponding to (iii)–(v) were performed within the same FOV for islands produced by stamp-off of a 50 μg/mL continuous field. Scale bars = 2 μm. Error bars are ± standard error of the mean from four independent substrate preparations. Details of the on island and area average intensity quantification are provided in the Electronic Supplementary Material.

that stamp-off from a high content uniform field produced islands with a global area average equivalent to a low content uniform field.

For our experimental geometry and inking process, we identified that FN-saturated stamps (inking concentration in excess of 30 μg/mL) could be stamped-off to produce islands resulting in a global density equivalent to that of a uniformly inked 2 μg/mL stamp (Fig. 2a, shaded region). This set of conditions straddled the adhesive threshold (44% relative to saturation, denoted by the dotted lines in Fig. 2) that we previously identified[12] as the critical density below which the keratocyte-like phenotype occurs, but above which the amoeboid phenotype occurs.

Quantitative fluorescence microscopy was used to measure the densities of FN on islands (Fig. 2c), over the area average (Fig. 2d), and between islands (Fig. 2e) after printing. We found that printed islands had densities (Fig. 2biii) comparable to that of continuous fields of high protein content (Fig. 2bi), while the protein content between islands was nearly zero (Fig. 2bv). The protein content of 2 μg/mL continuous fields (Fig. 2bii) and the area average protein content of islands (Fig. 2biv) were both below the critical density threshold. For each condition, 10–12 fields of view were acquired from each of four independent substrates.

Neutrophils Integrate Adhesive Stimulation Across Entire Contact Interface

We previously published observations of a phenotypic switch in neutrophil shape and motility governed by adhesive density.[12] Here, consistent with those findings, we observed the amoeboid phenotype on uniform fields of high FN density (50 μg/mL) (Figs. 3a and 3d) and the keratocyte-like phenotype on uniform fields of low FN density (2 μg/mL) (Fig. 3b). Both high and low density continuous fields represented surfaces with uniform adhesive stimulation across the cell-substrate interface. By contrast, our hybrid island surfaces presented the cells with two effective adhesive length scales simultaneously. On the scale of single islands the density was high, comparable to that of high protein-content uniform fields. On average across the scale of multiple islands, the density was low, comparable to that of low protein-content fields. We hypothesized that if a neutrophil was sensitive to local density it would assume the amoeboid phenotype whereas if it was sensitive to global density, across its

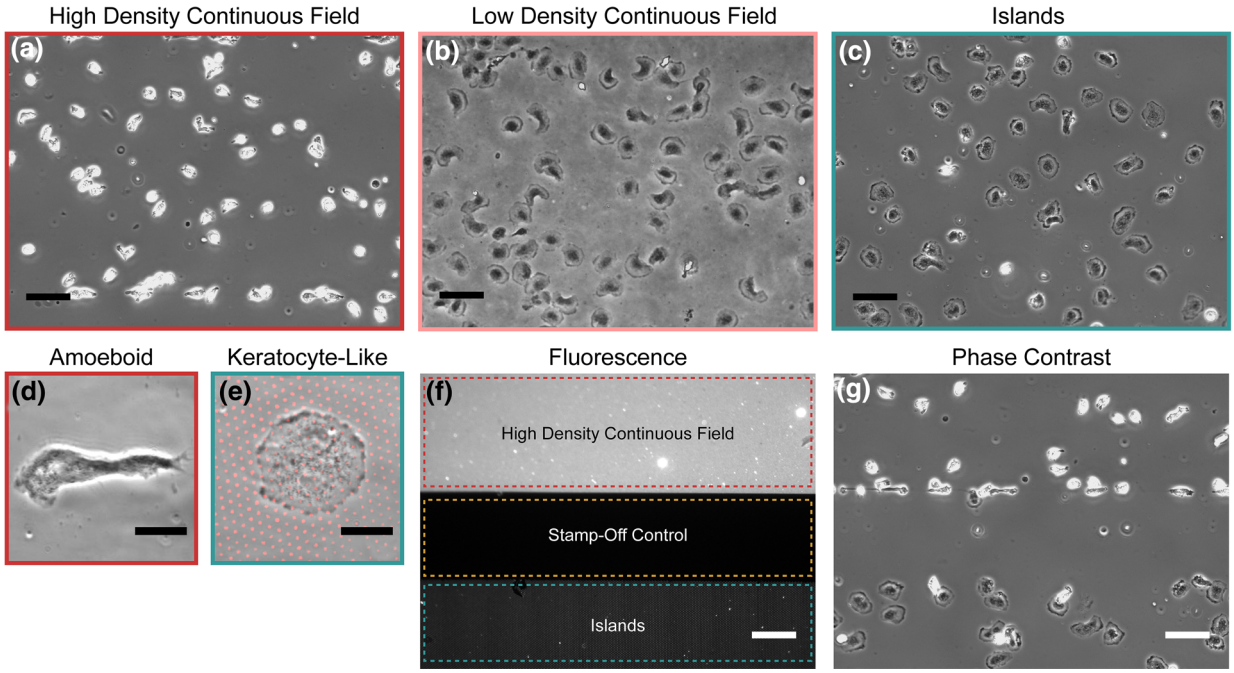

FIGURE 3. Neutrophils sense density at whole cell length scale. On continuous fields of FN neutrophils assume an (a) amoeboid phenotype on high density surfaces and a (b) keratocyte-like phenotype on low density surfaces. (c) However, on discrete islands, where local density is high and global density is low, neutrophils assume the keratocyte-like phenotype. Higher magnification images of (d) amoeboid phenotype on continuous field and (e) keratocyte-like phenotype on discrete islands where fluorescent signal has been superimposed. (f) Fluorescence image corresponding to FOV in (g). (g) Phase contrast image of neutrophils exhibiting amoeboid and keratocyte-like phenotypes in the same FOV with no adhesion in stamp-off control domain. Time lapse movie of neutrophil motility in (g) is supplied as Electronic Supplementary Movie S1. Scale bars = 50 μm for a, b, c, f, and g. Scale bars = 10 μm for d and e.

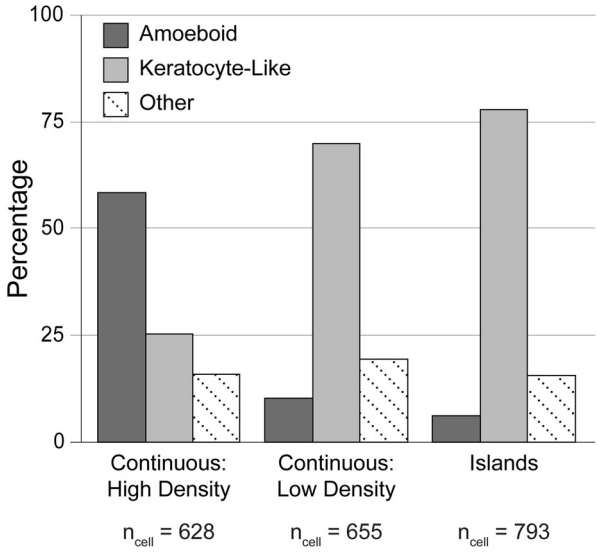

FIGURE 4. Phenotype frequency per experimental condition. Observed phenotypes for the three experimental conditions across all FOVs acquired were manually scored. On high density continuous fields the largest fraction was amoeboid (59%). On low density continuous fields and islands the largest fraction was keratocyte-like (70 and 78% respectively). Other denotes cells that were adherent but not spread or had ambiguous morphologies.

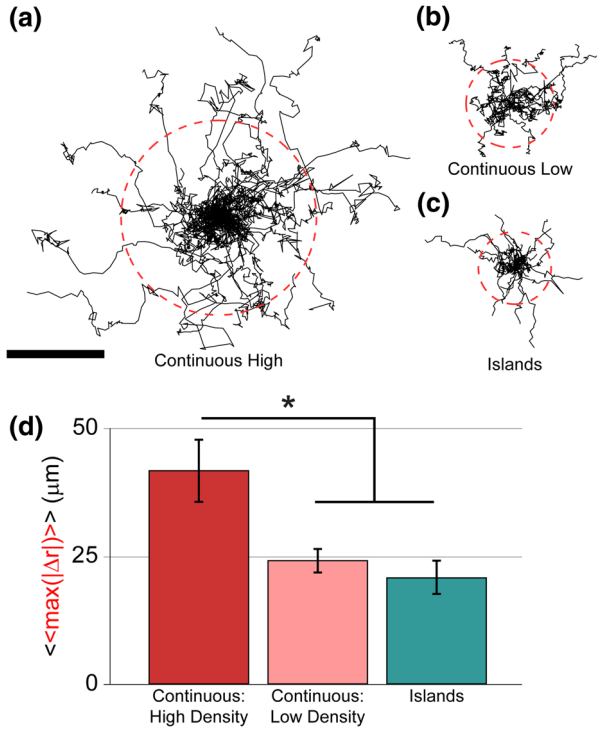

FIGURE 5. Neutrophil motility on islands is comparable to low density continuous fields. Cell trajectories through 30 min of motility from single representative experiments of (a) amoeboid motility on high density continuous fields, (b) keratocyte-like motility on low density continuous fields, and (c) keratocyte-like motility on hybrid islands. Scale bar = 50 μm. Dotted red circle is mean maximum displacement (<max(|Δr|)>) of set of 30 min trajectories. (d) Mean of the set of mean maximum displacements (≪max(|Δr|)≫) across all independent observations. Error bars are ± standard error of the mean ($N_{experiments/condition}$ = 6–7, $n_{cell/experiment}$ = 17–27). Asterisk denotes significant difference between populations as computed by *post hoc* Dunn-Sidak multiple comparisons method ($p < 0.05$).

contact interface, it would assume the keratocyte-like phenotype. Consistent with the later hypothesis, neutrophils assumed the keratocyte-like phenotype on engineered islands where the total protein content averaged over the cell contact interface was low (Figs. 3c and 3e). Both phenotypes were observable in the same field of view when a continuous field was adjacent to discrete islands (Fig. 3g). In Fig. 4 the phenotype scores for the three experimental conditions across all FOVs acquired are reported. On high density continuous fields the amoeboid phenotype predominates (59% amoeboid) while on low density continuous fields and islands, the keratocyte-like phenotype predominates (70 and 78% keratocyte-like respectively).

Additionally, we observed that neutrophils could exhibit a rapid change in motile phenotype. Neutrophils displaying the amoeboid phenotype on high density uniform fields could transform into the keratocyte-like phenotype within seconds when they moved from uniform fields to stamped-off islands whose overall ligand density was low. The movie corresponding to Fig. 3g is provided as Movie S1. There was a small degree of convective flow in the system that forced neutrophils across the non-adhesive domain between fields and islands. The non-adhesive domain served as an internal control and established that the residual protein content between islands (Fig. 2bv), generated in the same manner, was not sufficient to support adhesion. This can be concluded because the large non-adhesive band between the continuous field and island array was generated by stamp-off in a manner identical to that used in the interstitial space between islands.

Neutrophils maintain an amoeboid appearance while being pushed over the non-adhesive stamp-off control suggesting that the cells do not require continuous adhesive stimulation to maintain this polarized phenotype. However, neutrophils are not terminally committed to this polarized phenotype as they rapidly transition to the well-spread keratocyte-like phenotype upon arrival in the island domain.

Comparable Neutrophil Motility on Discrete Islands and Continuous Fields

After 30 min of motility, neutrophils undergoing amoeboid migration on high density uniform fields of

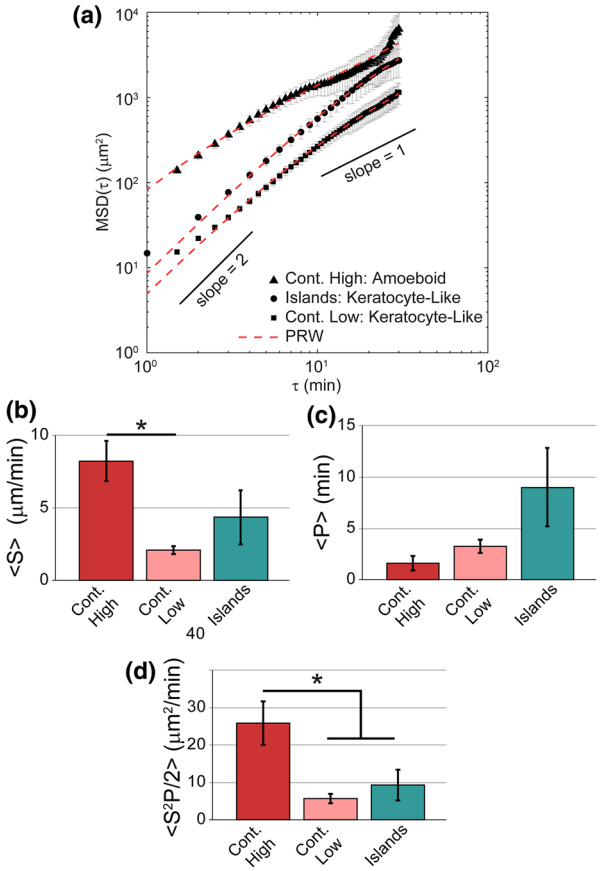

FIGURE 6. MSD analysis of neutrophil motility on islands and fields. (a) Mean squared displacements from single representative experiments for each condition. Dotted red line is fit of persistent random walk model (PRW) to empirical data. Mean of the set of model fit parameters (b) speed, (c) persistence, and (d) the random motility coefficient for all independent observations. Error bars are ± standard error of the mean ($N_{experiments/condition}$ = 6–7, $n_{cell/experiment}$ = 36–42). Asterisk denotes significant difference between populations as computed by *post hoc* Dunn-Sidak multiple comparisons method ($p < 0.05$).

FN (Fig. 5a) achieve a greater net dispersal than their keratocyte-like counterparts on low density uniform fields (Fig. 5b) as well as hybrid islands (Fig. 5c). A metric of dispersal is the mean maximum displacement ($<\max(|\Delta r|)>$) of all trajectories after 30 min. Cell trajectories followed less than 30 min were excluded in this analysis to avoid biasing the means. The mean maximum displacement of keratocyte-like motility on low density continuous fields of FN and hybrid islands was statistically indistinguishable (Fig. 5d).

To assess the evolution of the motile cells we also computed mean squared displacements (MSD) as a function of time (Fig. 6a) and fit the curves with the persistent random walk model of cell kinesis ($<\Delta r^2(\tau)> = 2S^2P[\tau - P(1 - \exp(-\tau/P))]$)[11,15] in terms of the best-fit parameters speed (S, Fig. 6b), persistence time (P, Fig. 6c), and the random motility coefficient ($S^2P/2$, Fig. 6d). As a result of this analysis, we found the amoeboid cells move twice as fast, leading to their increased dispersion (Fig. 6b). Although there was no statistically significant difference in the directional persistence of the two phenotypes, we did see an increase in the distribution of persistence times of keratocyte-like neutrophils on islands (Fig. 6c). This observation may be a consequence of the discretized islands presenting the cells with limited directional degrees of freedom as compared to continuous adhesive fields. Finally, we observe a statistically significant increase in random motility coefficient for amoeboid migration relative to keratocyte-like migration, again consistent with the strong speed-squared dependence of the random motility coefficient.

DISCUSSION

We previously reported that the density of adhesive ligand dictates the shape and mode of neutrophil migration on equally stiff substrates.[12] In this paper, we explored if patterns of adhesive ligand could be used to induce changes in the phenotype of motility. To address this issue, we employed the stamp-off method of microcontact printing[10] and engineered adhesive environments to present neutrophils with two densities of adhesion molecules on two length scales simultaneously. By careful control of protein loading for a given geometry, we were able to achieve three different topologies that straddled the critical adhesive threshold (44% saturation) which delineated the keratocyte-like phenotype from the classical amoeboid phenotype. The three conditions explored were as follows: a continuous field of FN at high density (>44% saturation) known to elicit the amoeboid phenotype; a continuous field of FN at a low density (<44% saturation) known to elicit the keratocyte-like phenotype; and a hybrid island array where the ligand density on the islands was high but the area average density was low. On these hybrid adhesive surfaces, neutrophils robustly assumed the keratocyte-like phenotype, integrating the adhesive stimuli over their entire contact interface and responding as if the set of discrete islands were a continuous field.

The integration of distributed adhesive contact into a global cell response has been observed in a variety of mesenchymal cells[7,17] Lehnert and coworkers explored a large state space of island size and pitch in fibroblasts and melanoma cells and found that these cells spread on discrete islands of less than 1 μm^2 with pitch less than 5 μm as if they were continuous fields of protein. Likewise we observe that neutrophils spread and are motile on discrete islands of 0.55 μm^2 and 1.9 μm pitch as if they were continuous fields of low density protein.

However, the dramatic reduction in contact area that occurs when neutrophils assume the highly motile amoeboid phenotype is quite distinct from the behavior of mesenchymal cells on a high density of adhesion molecules. The reduced contact area of amoeboid neutrophils (~100 μm^2) is within the same order of magnitude as the actual total adhesive contact area of keratocyte-like neutrophils on islands (~100 islands/cell $\times$ 0.55 μm^2/island). Thus, the phenotypic switch in neutrophils could be driven by the cell's attempt to maintain a constant level of adhesive stimulation across its contact interface.

While the islands we employed in this study are submicron (diameter = 834 $\pm$ 55 nm), they are large compared to the lateral distance between adhesive ligand binding sites of 58–73 nm necessary to support integrin receptor clustering.[1] Clustering of β_2 (CD11b) integrins and the downstream cytoskeletal rearrangement that results is critical to the neutrophil's execution of terminal effector functions like reactive oxygen intermediate generation and proteolytic enzyme secretion.[23] We previously showed, using function blocking antibodies, that neutrophils utilize the promiscuous integrin receptor MAC-1 ($\alpha_M\beta_2$) to support haptokinetic migration on FN.[12] Therefore the appearance of the keratocyte-like phenotype on islands suggests neutrophils do not respond to adhesive ligand density on the length scale of a receptor cluster but rather integrate the total adhesive stimulus across all clusters.

The pursuit of adhesive stimulation across the contact interface may itself by the consequence of the cell attempting to maintain tensional homeostasis. Our lab has previously demonstrated that neutrophil traction stresses are highest in the rear uropod of motile amoeboid neutrophils.[24] This asymmetric rearward contractility is understood to be the mechanism by which the cytoplasm is propelled forward generating a protrusive force despite the contact footprint of the cell being quite small. This is in contrast to the behavior of less polarized mesenchymal cells which show a linear increase in traction generation as contact footprint increases.[28] Whereas the keratocyte-like phenotype presumably represents a state of high traction generation doing work against the substrate, the amoeboid phenotype represents a state of high traction generation doing work to deform the cell body itself. In neutrophils, these distinct states are archived on equally stiff substrates but elicited by the extent of adhesive stimulation imparted to the cell.

Neutrophils are central mediators of the body's inflammatory response to tissue trauma and infection, capable of pathogen clearance, cytokine secretion, reactive oxygen intermediate production and nuclear-extracellular trap formation.[3] Numerous chemical and physical cues guide neutrophil response to trauma and infection. Here we demonstrate that neutrophils are sensitive to adhesion ligand density, integrating adhesive stimulation across their entire contact interface to coordinate a whole-cell motile response. Additionally, our findings may have applicability to the study of cancer metastasis and specifically the epithelial to mesenchymal transition.[26,30] It has been established that tumor stiffening drives integrin clustering which supports the malignant cell phenotype.[22] Perhaps a concurrent increase in extracellular adhesivity of the stiff tumor microenvironment could subsequently induce a highly motile amoeboid-like transition in previously stationary malignancies. Future work in this area will involve extension of our studies to different topologies and physiologically relevant cell types.

ELECTRONIC SUPPLEMENTARY MATERIAL

The online version of this article (doi:10.1007/s10439-015-1408-2) contains supplementary material, which is available to authorized users.

ACKNOWLEDGEMENTS

We are grateful to Eric Johnston for laboratory assistance and Christopher S. Chen, PhD and Ravi A. Desai, PhD for their time and expertise in teaching us the stamp-off method of microcontact printing. Funding for this work was provided by a National Science Foundation Graduate Research Fellowship to SJH and grants from the National Institutes of Health (HL18208 and GM104287) to DAH.

REFERENCES

[1]Arnold, M., E. A. Cavalcanti-Adam, R. Glass, J. Blummel, W. Eck, M. Kantlehner, H. Kessler, and J. P. Spatz. Activation of integrin function by nanopatterned adhesive interfaces. *Chemphyschem* 5:383–388, 2004.

[2]Barnhart, E. L., K. C. Lee, K. Keren, A. Mogilner, and J. A. Theriot. An adhesion-dependent switch between mechanisms that determine motile cell shape. *PLoS Biol.* 9:e1001059, 2011.

[3]Borregaard, N. Neutrophils, from marrow to microbes. *Immunity* 33:657–670, 2010.

[4]Cassimeris, L., H. McNeill, and S. H. Zigmond. Chemoattractant-stimulated polymorphonuclear leukocytes contain two populations of actin filaments that differ in their spatial distributions and relative stabilities. *J. Cell Biol.* 110:1067–1075, 1990.

[5]Charras, G., and E. Sahai. Physical influences of the extracellular environment on cell migration. *Nat. Rev. Mol. Cell Biol.* 15:813–824, 2014.

[6]Chen, C. S., J. L. Alonso, E. Ostuni, G. M. Whitesides, and D. E. Ingber. Cell shape provides global control of focal

adhesion assembly. *Biochem. Biophys. Res. Commun.* 307:355–361, 2003.
[7]Chen, C. S., M. Mrksich, S. Huang, G. M. Whitesides, and D. E. Ingber. Geometric control of cell life and death. *Science* 276:1425–1428, 1997.
[8]Crocker, J. C., and B. D. Hoffman. Multiple-particle tracking and two-point microrheology in cells. *Cell Mech.* 83:141–178, 2007.
[9]Desai, R., M. Yang, N. Sniadecki, W. Legant, and C. S. Chen. Microfabricated post-array-detectors (mPADs): an approach to isolate mechanical forces. *J. Vis. Exp.* 7:311, 2007.
[10]Desai, R. A., M. K. Khan, S. B. Gopal, and C. S. Chen. Subcellular spatial segregation of integrin subtypes by patterned multicomponent surfaces. *Integr. Biol.* 3:560–567, 2011.
[11]Dunn, G. A. Characterising a kinesis response: time averaged measures of cell speed and directional persistence. *Agents Actions Suppl.* 12:14–33, 1983.
[12]Henry, S. J., J. C. Crocker, and D. A. Hammer. Ligand density elicits a phenotypic switch in human neutrophils. *Integr. Biol.* 6:348–356, 2014.
[13]Jannat, R. A., G. P. Robbins, B. G. Ricart, M. Dembo, and D. A. Hammer. Neutrophil adhesion and chemotaxis depend on substrate mechanics. *J. Phys.-Condens. Matter* 22:194117, 2010.
[14]Lammermann, T., B. L. Bader, S. J. Monkley, T. Worbs, R. Wedlich-Soldner, K. Hirsch, M. Keller, R. Forster, D. R. Critchley, R. Fassler, and M. Sixt. Rapid leukocyte migration by integrin-independent flowing and squeezing. *Nature* 453:51–55, 2008.
[15]Lauffenburger D. A., and J. J. Linderman. Receptors: Models for Binding, Trafficking, and Signaling. New York: Oxford University Press, 1993, p. x, p. 365.
[16]Lee, J., and K. Jacobson. The composition and dynamics of cell-substratum adhesions in locomoting fish keratocytes. *J. Cell Sci.* 110(Pt 22):2833–2844, 1997.
[17]Lehnert, D., B. Wehrle-Haller, C. David, U. Weiland, C. Ballestrem, B. A. Imhof, and M. Bastmeyer. Cell behaviour on micropatterned substrata: limits of extracellular matrix geometry for spreading and adhesion. *J. Cell Sci.* 117:41–52, 2004.
[18]Ley, K., C. Laudanna, M. I. Cybulsky, and S. Nourshargh. Getting to the site of inflammation: the leukocyte adhesion cascade updated. *Nat. Rev. Immun.* 7:678–689, 2007.
[19]McDonald, B., K. Pittman, G. B. Menezes, S. A. Hirota, I. Slaba, C. C. M. Waterhouse, P. L. Beck, D. A. Muruve, and P. Kubes. Intravascular danger signals guide neutrophils to sites of sterile inflammation. *Science* 330:362–366, 2010.
[20]Nathan, C. Neutrophils and immunity: challenges and opportunities. *Nat. Rev. Immunol.* 6:173–182, 2006.
[21]Oakes, P. W., D. C. Patel, N. A. Morin, D. P. Zitterbart, B. Fabry, J. S. Reichner, and J. X. Tang. Neutrophil morphology and migration are affected by substrate elasticity. *Blood* 114:1387–1395, 2009.
[22]Paszek, M. J., N. Zahir, K. R. Johnson, J. N. Lakins, G. I. Rozenberg, A. Gefen, C. A. Reinhart-King, S. S. Margulies, M. Dembo, D. Boettiger, D. A. Hammer, and V. M. Weaver. Tensional homeostasis and the malignant phenotype. *Cancer Cell* 8:241–254, 2005.
[23]Raptis, S. Z., S. D. Shapiro, P. M. Simmons, A. M. Cheng, and C. T. Pham. Serine protease cathepsin G regulates adhesion-dependent neutrophil effector functions by modulating integrin clustering. *Immunity* 22:679–691, 2005.
[24]Smith, L. A., H. Aranda-Espinoza, J. B. Haun, M. Dembo, and D. A. Hammer. Neutrophil traction stresses are concentrated in the uropod during migration. *Biophys. J.* 92:L58–L60, 2007.
[25]Stroka, K. M., and H. Aranda-Espinoza. Neutrophils display biphasic relationship between migration and substrate stiffness. *Cell Motil Cytoskeleton* 66:328–341, 2009.
[26]Thiery, J. P., H. Acloque, R. Y. J. Huang, and M. A. Nieto. Epithelial-mesenchymal transitions in development and disease. *Cell* 139:871–890, 2009.
[27]Vogel, V., and M. Sheetz. Local force and geometry sensing regulate cell functions. *Nat. Rev. Mol. Cell Biol.* 7:265–275, 2006.
[28]Wang, N., E. Ostuni, G. M. Whitesides, and D. E. Ingber. Micropatterning tractional forces in living cells. *Cell Motil Cytoskeleton* 52:97–106, 2002.
[29]Yang, M. T., J. Fu, Y. K. Wang, R. A. Desai, and C. S. Chen. Assaying stem cell mechanobiology on microfabricated elastomeric substrates with geometrically modulated rigidity. *Nat. Protoc.* 6:187–213, 2011.
[30]Yao, D., C. Dai, and S. Peng. Mechanism of the mesenchymal-epithelial transition and its relationship with metastatic tumor formation. *Mol. Cancer Res.* 9:1608–1620, 2011.
[31]Ziebert, F., and I. S. Aranson. Effects of adhesion dynamics and substrate compliance on the shape and motility of crawling cells. *PLoS One* 8:e64511, 2013.
[32]Zigmond, S. H. Chemotaxis by polymorphonuclear leukocytes. *J. Cell Biol.* 77:269–287, 1978.

Electronic Supplementary Material
Henry et al. Motile human neutrophils sense ligand density over their entire contact area

Fluorescence Images as Acquired

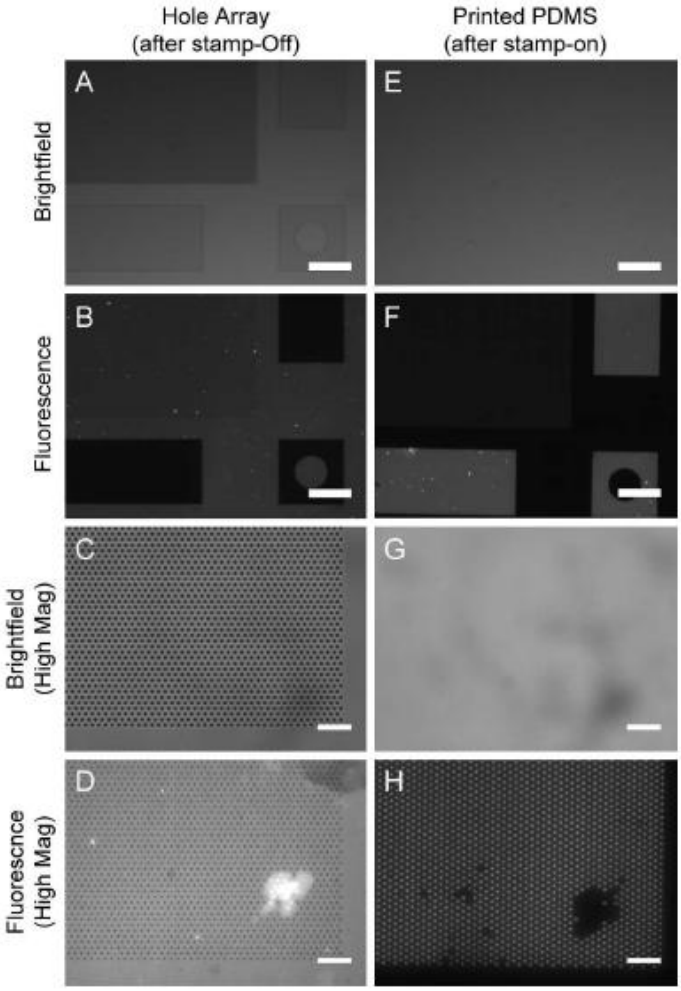

Figure S1. Stamp-off method of microcontact printing to generate discrete islands: no contrast enhancement. (*A*) Brightfield image of hole array used in stamp-off procedure. (*B*) Fluorescence image of protein on hole array after stamp-off. (*C*) and (*D*) are higher magnification images of *A* and *B* features respectively. (*E*) Brightfield image of PDMS coverslip after stamp-on procedure. (*F*) Fluorescence image of protein on flat PDMS coverslip after stamp-on. (*G*) and (*H*) are higher magnification images of *C* and *D* features respectively. For a given magnification, fluorescence images were captured identically. Scalebars = 200 μm for *A*, *B*, *E*, and *F*. Scalebars = 10 μm for *C*, *D*, *G*, and *H*.

Electronic Supplementary Material
Henry et al. Motile human neutrophils sense ligand density over their entire contact area

Determination of Island Diameter

To measure the printed island diameter after stamp-off in an intensity-independent manner we performed a full width at half maximum (FWHM) analysis on the raw fluorescence images. The histogram of FWHM values from 40 measurements (5 islands from each of 2 different fields of view (FOV) from each of four different printed substrates) is reported in Fig. S2 *A*. As the variation within a FOV was comparable to the variation across FOVs (Fig. S2 *B*) we considered the mean of the ensemble of FWHM values to be the in-focus value (m ± sd = 825 ± 63 nm).

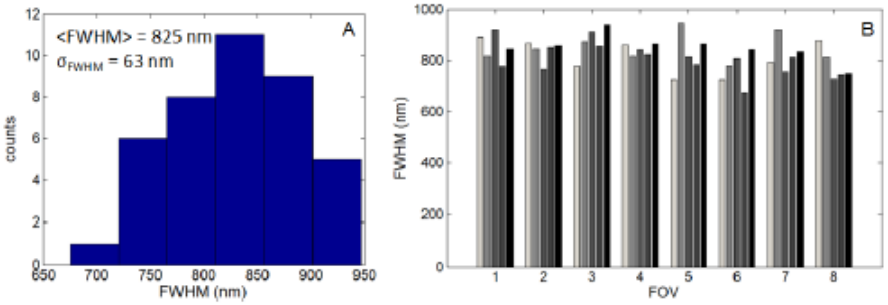

Figure S2. Full Width at Half Maximum (FWHM) Analysis. (*A*) Histogram of 40 FWHM measurements. (*B*) Variation within a single field-of-view (FOV) was on the order of that observed across all FOVs suggesting independent FOVs were equivalently focused.

To understand how FWHM varied as a function of the actual (i.e. pre-convolved) island diameter in a diffraction limited system we performed a numerical two-dimensional convolution of an island with uniform intensity (i.e. 100%) by a normalized Gaussian with zero mean and standard deviation = 101.2 nm. This Gaussian was a best-fit approximation to the core of an Airy disk having a first intensity minimum at radius = 289.5 nm. This radius corresponds to the resolution limit of our microscope as defined by the Rayleigh Criterion (radius = 0.61*λ/NA) where $\lambda_{AlexaFluor594}$ = 617 nm and $NA_{100X,oil}$ = 1.3. The result of a series of numerical convolutions is reported in Figure S3. Fitting the FWHM vs. actual island diameter curve with a polynomial allowed us to infer the pre-convolved diameter of our islands given the mean empirical FWHM previously computed. In this manner we determined the island diameter to be 834 ± 55 nm (m ± sd).

Electronic Supplementary Material
Henry et al. Motile human neutrophils sense ligand density over their entire contact area

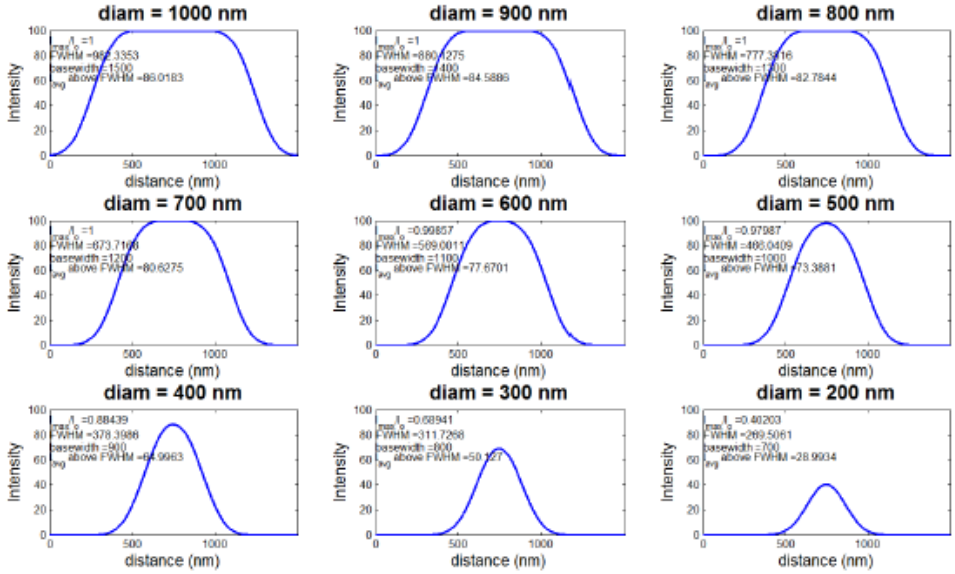

Figure S3. Numeric Convolution Study. Results of a series of two dimensional convolutions of a normalized Guassian approxiamation to a diffraction limited Airy disk (standard deviation = 101.2 nm) with islands of uniform (i.e. 100%) intensity.

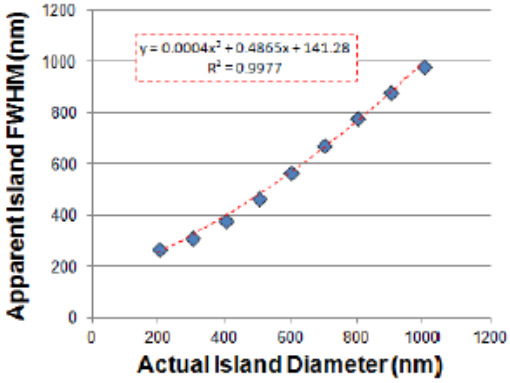

Figure S4. FWHM vs. Actual Island Diameter. Best fit second order polynomial for simulated FWHM as a function of actual (i.e. pre-convolution) island diameter.

Determination of Island Pitch

To quantify array pitch, fluorescence images (Fig. S5 *C*) were processed in MATLAB by performing a Canny edge detection and object fill (Fig. S5 *D*). The pitch for an array was determined by computing the mean six nearest neighbor distance for islands having six nearest neighbors (i.e. excluding edge islands) (Fig. S5 *E*).

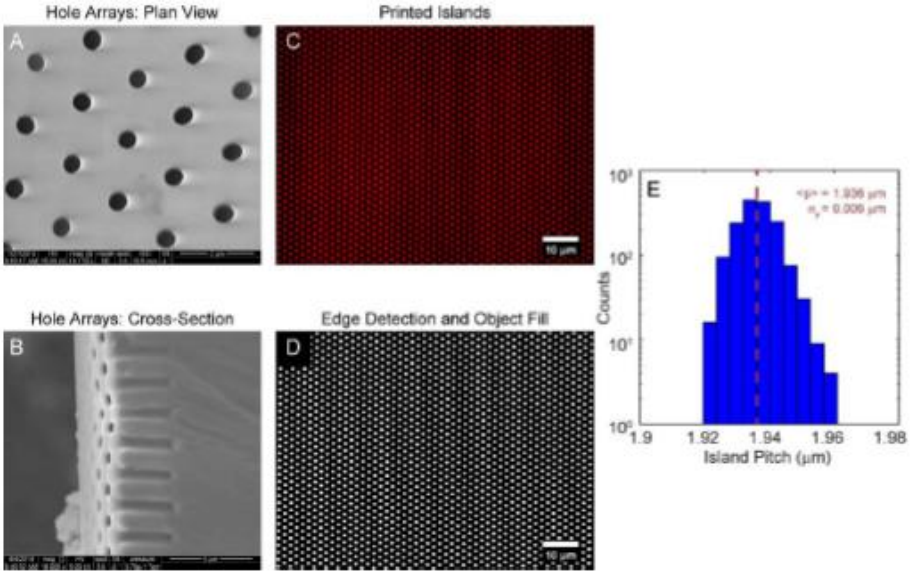

Figure S5. Measurement of printed island pitch. Scanning electron micrograph (*A*) plan view and (*B*) cross-section view of PDMS hole arrays used in stamp-off procedure. (*C*) Fluorescence image of printed islands and its (*D*) corresponding binary bitmap after image processing to measure island positions. (*F*) Histogram of nearest neighbor distances (i.e. pitch) in *D*. The pitch quoted in the main text are the mean and standard error from five samples, analyzed in the same manner as above.

Determination of Intensity Correction Factor

When quantitatively comparing the intensity of a single island to that of a continuous field of protein, we have to account for an apparent reduction in intensity due to the resolution limit of our microscope. In addition to modeling how FWHM varies as a function of the actual island diameter (Fig. S3) we can also model how the average intensity of an island decreases as a function the actual island diameter. After numerical convolution we computed the average intensity of the portion of the convolved image that resides within the FWHM diameter (Fig. S6) which is approximately equal to the diameter of the manual circular ROIs set when computing the empirical on island average intensity. For our system an apparent decrease in intensity of 12

± 1 % occurs. Thus to correct for this apparent reduction in intensity we divided the average empirical intensity measurement by 0.88 in the on island and area average metrics (Fig. S7). It is important to note that even before this correction was applied the on island and area average metrics straddled the critical adhesive threshold of 44% relative to saturation. This threshold was previously found to delineate the keratocyte-like and amoeboid morphologies in human neutrophils on continuous fields of protein.

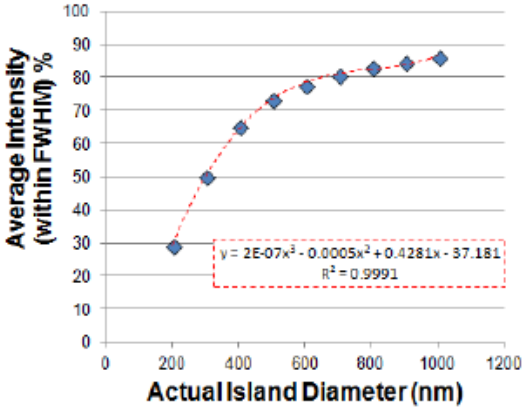

Figure S6. Average Island Intensity vs. Actual Island Diameter. Best fit third order polynomial for simulated average intensity (within FWHM) as a function of actual (i.e. pre-convolution) island diameter.

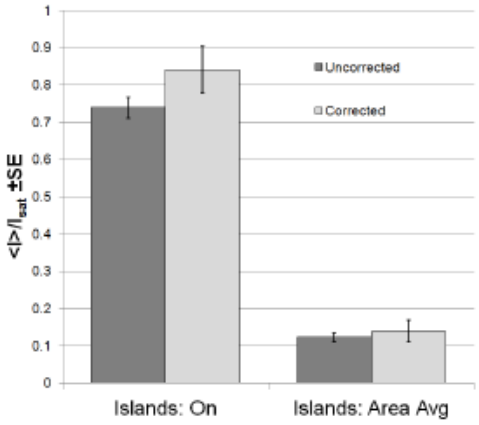

Figure S7. Intensity Correction of Island Measurements. To correct for an apparent reduction in island intensity due to the resolution limit of our microscope the on island and area average metrics were divided by 0.88 (i.e. unity minus the average modeled intensity reduction). Even before correction, the two metrics straddled the critical adhesive threshold of 44 % (relative to saturation) which delineated the keratocyte-like and amoeboid phenotypes.

Electronic Supplementary Material
Henry et al. Motile human neutrophils sense ligand density over their entire contact area

Determination of Island Area Fraction Relative to a Continuous Field

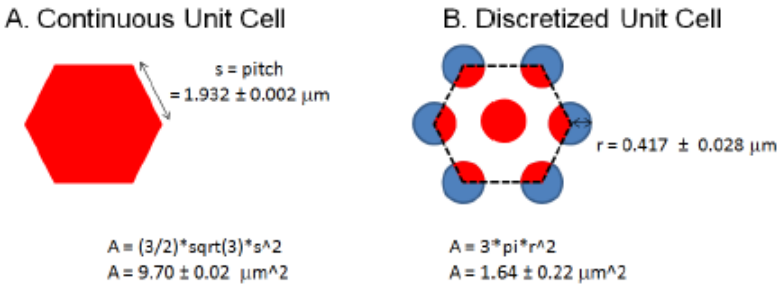

$A_{islands}/A_{continuous}$ = 1.64/9.70 = 17 ± 2 %

Figure S8. Area Computation. (*A*) Continuous unit hexagon with side length of empirically measured pitch. (*B*) Discretized unit hexagon with islands of empirically measured radius. Error propagation was used to compute standard deviations corresponding to the area and fractional area calculations.